RESEARCH ARTICLE | MAY 25 2023

On the possible locus of the liquid–liquid critical point in real water from studies of supercooled water using the TIP4P/Ice model FREE

Jorge R. Espinosa; Jose Luis F. Abascal; Lucia F. Sedano; ... et. al

Check for updates

View Online

Export Citation

CrossMark

On the possible locus of the liquid–liquid critical point in real water from studies of supercooled water using the TIP4P/Ice model

View Online   Export Citation   CrossMark

Jorge R. Espinosa,[1,2] (ID) Jose Luis F. Abascal,[1] (ID) Lucia F. Sedano,[1] (ID) Eduardo Sanz,[1] (ID) and Carlos Vega[1,a] (ID)

AFFILIATIONS

[1] Department of Chemical Physics, Faculty of Chemical Sciences, Universidad Complutense de Madrid, 28040 Madrid, Spain
[2] Cavendish Laboratory, Department of Physics, Maxwell Centre, University of Cambridge, J Thomson Avenue, Cambridge CB3 0HE, United Kingdom

[a]Author to whom correspondence should be addressed: cvega@quim.ucm.es

ABSTRACT

One of the most accepted hypothesis to explain the anomalous behavior of water is the presence of a critical point between two liquids, the liquid–liquid critical point (LLCP), buried within the deep supercooled regime. Unfortunately, such hypothesis is hard to be experimentally confirmed due to fast freezing. Here, we show that the TIP4P/Ice water potential shifted by 400 bar can reproduce with unprecedented accuracy the experimental isothermal compressibility of water and its liquid equation of state for a wide pressure and temperature range. We find, both by extrapolation of response function maxima and by a Maxwell construction, that the location of the model LLCP is consistent with previous calculations. According to the pressure shift needed to recover the experimental behavior of supercooled water, we estimate the experimental LLCP to be located around 1250 bar and 195 K. We use the model to estimate the ice nucleation rate (J) in the vicinity of the hypothesized LLCP experimental location and obtain $J = 10^{24}$ m^{-3} s^{-1}. Thereby, experiments where the ratio between the cooling rate and the sample volume is equal or larger than the estimated nucleation rate could probe liquid–liquid equilibrium before freezing. Such conditions are not accessible in common experiments with microdroplets cooled at a few kelvin per second, but they could be, for instance, using nanodroplets of around 50 nm radius observed in a millisecond timescale.

Published under an exclusive license by AIP Publishing. https://doi.org/10.1063/5.0147345

I. INTRODUCTION

In order to deeply understand the fascinating anomalous behavior of water, it is necessary to explore the supercooled regime.[1] However, when liquid water is supercooled below its melting temperature, freezing can occur since ice Ih is the thermodynamically stable phase. Impurities in water promote the formation of ice nuclei that, once they reach a certain critical size, induce irreversible ice growth.[2–4] Nevertheless, in the absence of impurities, liquid water can remain metastable for a certain time depending on the applied temperature and pressure as well as on the sample size. Importantly, to achieve large supercooling, the sample needs to be as small as possible since the time required to obtain a critical nucleus (in the absence of impurities) increases with the inverse of the system volume. Despite the multiple experimental challenges required to overcome spontaneous freezing,[5] ultra-pure water nanoscopic droplets have been shown to remain liquid up to 70 K of supercooling at ambient pressure[6–8] and up to 92 K of supercooling at high pressures (i.e., 2000 bar) using microdroplets.[9] Remarkably, experiments of this kind[10–16] have motivated an extensive list of studies elucidating the phase behavior of supercooled water before freezing takes place.

In 1973, the first evidence of supercooled water having anomalous response functions was reported by Angell and Tucker.[17] At room pressure, the isobaric heat capacity (C_p) was shown to monotonically increase up to 38 K of supercooling, where spontaneous freezing was inevitable. Later on, other thermodynamic response functions, such as the isothermal compressibility (κ_T)[18] or the thermal expansion coefficient (α_P),[19] have been shown to apparently diverge at ambient pressure as temperature decreases up to ~40 K of supercooling. However, more recent experiments reaching lower temperatures (i.e., ~228 K) by means of state-of-the-art X-ray

experiments have shown that both C_p[20] and κ_T[21,22] do not actually diverge at ambient pressure but instead reach a maximum value around 229 K. Another characteristic water anomaly is its density maximum (at around 277 K at ambient pressure) and the possible existence of a minimum, which is thought to be within the deep supercooled regime according to small-angle neutron scattering experiments of heavy water under confinement.[23]

Since direct experimental observations are difficult to obtain—especially as one dives into the supercooled region[24]—computer simulations have emerged as a powerful tool to investigate supercooled water.[25–27] The main advantages that computer simulations possess with respect to experiments are (1) the inherent simplicity to prepare pure water systems with no interfaces (under periodic boundary conditions); (2) the small size and timescales, which are extraordinarily convenient for avoiding spontaneous freezing; and (3) the ease for extracting thermodynamic, structural, and molecular information. On the other hand, the main drawback of classical simulations is that the results are affected by the choice of an approximate interaction potential (even quantum calculations rely on an approximated functional, and moreover, only including nuclear quantum effects would enable to reproduce the experimental properties of water). Therefore, simulation predictions should always be tested with experiments. In the past few years, a great effort has been dedicated to improve the accuracy of water models.[28–35] Coarse-grained models,[35,36] *ab initio* potentials,[34,37] classical polarizable[32,33] and non-polarizable (both rigid and flexible) force fields[28–31,38] have been extensively used to investigate the properties of ice and supercooled water.[39–43] It is certainly true that some models deviate less from the experimental behavior than others. In this work, we shall show that this is indeed the case when focusing on the properties of supercooled water.

In 1992 the pioneering simulation study of Poole *et al.*[25] suggested the possible existence of a liquid–liquid critical point (LLCP) which would largely explain water anomalies.[25] Several water potentials—including the ST2,[44–47] mW,[48,49] WAIL,[50] TIP4P/2005,[26,51] and TIP4P/Ice[26,52–54]—have been used to investigate the existence and precise location of the LLCP. With the exception of the mW model of water for which no liquid–liquid transition has been found,[48,49] for many other water models, such as the ST2,[44–47] TIP4P/2005,[26,55–59] TIP4P/Ice,[26,52–54,60] or WAIL,[50] strong evidence points out the presence of such transition. This has been further confirmed by rigorous methods for ST2,[46] TIP4P/Ice, and TIP4P/2005.[26] Claims on the lack of such transition for ST2[48] and TIP4P/2005[49] were based on calculations including a mistake in the initial velocities of the Hybrid Monte Carlo method as they did not satisfy the Maxwell–Boltzmann distribution, thus yielding incorrect results.[47,61] For the TIP4P/2005, a number of studies have shown clear evidence of a liquid–liquid transition at low temperatures[26,51,55–59] (with the only exception of a recent study[62] are still pending on validation by independent calculations).

In parallel, polarizable potentials, such as the MB-pol,[63] iAMOEBA,[64] or WAIL[50] as well as density functional *ab initio* models (using the SCAN functional) optimized with neural networks[65] have been shown to exhibit signatures of a liquid–liquid transition. Nevertheless, for this new generation of polarizable and "first-principles" models, it is computationally very demanding to

precisely determine the location of the LLCP.[66] In this respect, guidance from simpler yet reliable models is highly valuable.[61,67]

The TIP4P/2005 model describes quite well the properties of supercooled water.[68] However, the increase in compressibility with supercooling at room pressure is less steep than in experiments. A few years ago, we showed that this property is better described by the TIP4P/Ice potential.[69] In this work, we go a step further and show that the TIP4P/Ice model closely reproduces the experimental behavior of supercooled water upon applying a 400 bar pressure shift on its predicted properties. Qualitatively, one could understand the pressure shift as an effective way to induce the hydrogen bond network disruption caused by nuclear quantum effects although this is just a possible speculative explanation.

We focus on the ability of the model to predict thermodynamic properties, such as the isothermal compressibility and the liquid equation of state (EOS) as well as structural information, such as g_2, the height of the second peak of the oxygen–oxygen radial distribution $[g_{O-O}(r)]$, or A_2, the integral of the $g_{O-O}(r)$ second peak. Once demonstrated the success of the pressure-shifted model to reproduce experimental properties, we verify the existence and location of a LLCP by both a Maxwell construction and by evaluating the maxima of the response functions (C_p and κ_T), which are spread out away from the critical point but converge with the Widom line (the maxima of the correlation length) in its vicinity. The predicted locus for the TIP4P/Ice LLCP matches previous estimations.[26,52] Importantly, the pressure shift suggests a possible location for the LLCP in real water around 195 K and 1250 bar. There have been many attempts to infer the LLCP locus,[70–74] and we hope that such search can be narrowed down with the guidance of the pressure-shifted TIP4P/Ice model.

Finally, we assess the possibility of experimentally probing the hypothesized LLCP locus before ice nucleates. For that purpose, we use the model to obtain ice nucleation rates (J) and obtain $J = 10^{24}$ m^{-3} s^{-1} in the LLCP surroundings. Thereby, to measure supercooled liquid properties before ice nucleation occurs in such region, one needs to keep the ratio between the cooling rate and the sample volume equal or larger than the estimated nucleation rate. That could be achieved, for instance, by using drops of about 50 nm radius (containing tens of millions of molecules) and observation timescales of milliseconds. Nevertheless, it remains to be determined whether the surface or the bulk dominates the behavior of such small drops. Should the bulk dominate, a narrow window for experimentally probing the water LLCP would remain open.

II. RESULTS AND DISCUSSION

A. TIP4P/Ice computational details

We model water with the TIP4P/Ice model,[31] an accurate non-polarizable rigid potential, which has been shown to provide outstanding predictions of the solid and supercooled liquid properties of water, including the phase diagram[31,75] equations of state,[31,69] ice growth, and nucleation rates[69] as well as interfacial free energy for the ice Ih–water interface.[76] For consistency with previous TIP4P/Ice nucleation and supercooled water computational studies,[26,52,53,69,77,78] we set the potential cutoff at 9 Å, and long-range Coulombic interactions are treated with Particle-Mesh-Ewald (PME) summations[79] using a relative error in forces of 10^{-5}. Long-range corrections to the Lennard-Jones part of the potential

in energy and pressure are also applied. We keep the O–H bond length and H–O–H angle values constant with the LINCS algorithm.[80] Simulations are performed with the GROMACS molecular dynamics package[81] (version 4.6.7) both in the NVT ensemble (with N equal to the number of particles, V the volume, and T the temperature), keeping T constant with the v-rescale thermostat,[82] and in the NpT ensemble, fixing pressure (p) with the Parrinello–Rahman barostat.[83] We integrate the equations of motion using the velocity-Verlet integrator. The chosen simulation timestep is 2 fs, and the relaxation time of the thermostat and barostat is 1.87 and 1.79 ps, respectively. The slightly different relaxation times for the thermostat and barostat have been intentionally chosen to avoid coupling between temperature and pressure fluctuations. Simulations typically lasted 1–2 μs, being those for the lower temperatures and higher pressures (i.e., below 205 K and over 1400 bar) of up to 8 μs for the biggest system (i.e., 2000 molecules), whereas for high temperatures ($T > 235$ K) simulations of roughly 500 ns where performed. For the lowest temperatures, the first 500–1500 ns are considered as equilibration time depending on each case. System sizes of 500 and 2000 water molecules are used as specified along the article. For further details on the TIP4P/Ice intermolecular potential, we refer the reader to the original model Ref. 31.

B. Isothermal compressibility and equation of state through different water potentials

To illustrate the current situation of some of the most common water force fields employed to investigate liquid–liquid immiscibility, we shall focus on two characteristic properties of liquid water: the isothermal compressibility (κ_T) and the liquid EOS, both of which have been experimentally measured up to moderate supercooling.[18,21,84,85] The isothermal compressibility is defined as

$$\kappa_T = -\frac{1}{V}\left(\frac{\partial V}{\partial p}\right)_T. \tag{1}$$

It can be evaluated by the derivative of the equation of state [i.e., Eq. (1)] or through the well-known fluctuation expression in the NpT ensemble,

$$\kappa_T = \frac{\langle V^2 \rangle - \langle V \rangle^2}{k_B T \langle V \rangle}, \tag{2}$$

where k_B refers to the Boltzmann constant and V refers to the system volume. In Fig. 1, we depict experimental data (orange symbols) for the isothermal compressibility [Panel (a)], and the liquid EOS [Panel (b)] compared to computational predictions from different water potentials including the mW,[36,86] SPC/E,[87–89] TIP4P/2005,[88] TIP4P/Ice [this work; evaluated through Eq. (2)], iAMOEBA,[64,90] and MB-pol.[63] As it can be seen, whereas κ_T as a function of T is accurately predicted by the MB-pol [Fig. 1(a), pink curve, referring to the $N = 512$ molecule system from Ref. 63], the liquid density and the temperature of maximum density (TMD) for this model deviate from the experimental measurements [Fig. 1(b)]. In contrast, the TIP4P/2005 model successfully reproduces the liquid EOS [Fig. 1(b), red curve] but underestimates the increase in compressibility as a function of supercooling [Fig. 1(a)]. In close resemblance to the TIP4P/2005 non-polarizable rigid potential, the polarizable iAMOEBA force field reproduces the liquid EOS despite significantly underestimating the isothermal compressibility [Fig. 1(a), light green curve]. The mW (dark green curve) and SPC/E (maroon curve) potentials provide a worse representation of the two magnitudes under scrutiny when compared to the experimental results. Finally, the TIP4P/Ice potential, despite moderately underestimating the liquid density with respect to experimental measurements as well as with respect to the TIP4P/2005 and iAMOEBA models, provides a slightly better representation of the maximum in compressibility compared to the two aforementioned models [Fig. 1(a), blue curve].

Interestingly, Fig. 1(b) shows an offset between the experimental trend of liquid density as a function of temperature and that predicted by the TIP4P/Ice model. That is, both curves remain fairly parallel to each other separated by a density shift of roughly 0.015 g/cm^3 across most of the studied temperatures. Since the density of water increases with pressure, one may wonder if the EOS of the TIP4P/Ice at higher pressure could reproduce the experimental densities at 1 bar. In Sec. II C, we shall discuss the implications of a
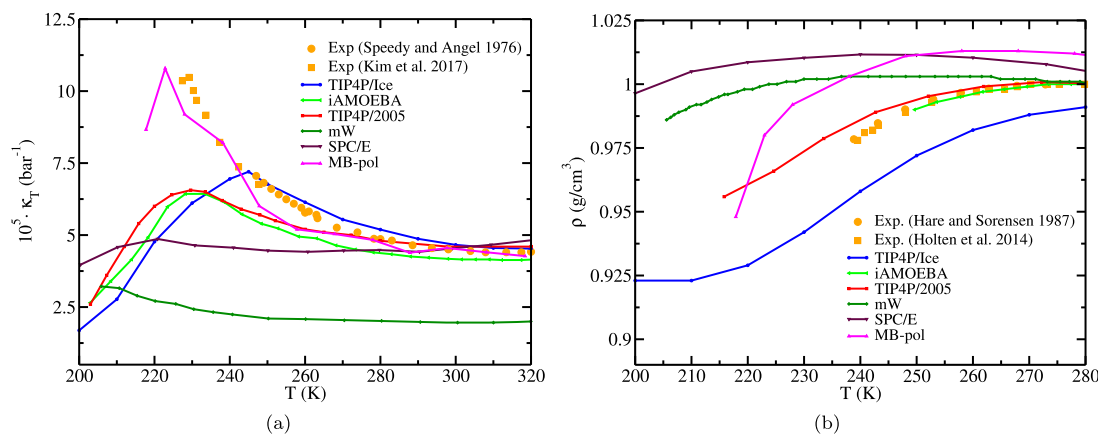
FIG. 1. Isothermal compressibility (a) and liquid density (b) as a function of temperature at room pressure from experimental measurements (orange symbols)[18,21,84,85] and for different water potentials[36,63,64,86–90] as indicated in the legend. Only the results for the TIP4P/Ice model have been obtained in this study.

pressure shift on the comparison between the TIP4P/Ice and water experimental phase behavior.

## C. A pressure shift on the TIP4P/Ice potential greatly improves its description of supercooled water

According to the results shown in Fig. 1, none of the most popular water models employed to investigate liquid–liquid criticality can quantitatively describe the dependence of both compressibility and liquid density with temperature at ambient pressure. Motivated by the constant density offset of the TIP4P/Ice model, we check if a pressure shift improves its description of both magnitudes. Regarding the compressibility, we find that a pressure shift of *circa* 400 bar recovers $\kappa_T(T)$ not only at ambient pressure but also at higher pressures [Fig. 2(a)]. The shift implies that experimental properties at a pressure p and temperature T are compared to TIP4P/Ice results at a pressure of $p + 400$ bar and the same temperature T. Despite the lack of experimental data under conditions of deep supercooling and high pressure, the remarkable agreement at higher temperatures for the different studied isobar suggests that the experimental maxima in κ_T might not be far away from those predicted by the pressure-shifted model. Importantly, we note that the compressibility becomes up to eight times larger at the maximum of the model at 1400 bar (i.e., 1000 bar for real water) as compared to that at room temperature.

We now test if the pressure shift on the TIP4P/Ice model also improves the description of the isobaric heat capacity. In Fig. 2(b), we compare experimental results for C_p at normal pressure[91,92] against predictions of the TIP4P/Ice potential at 1 and 400 bar. As can be seen, a significant improvement in the prediction of C_p can be achieved after applying the pressure shift on the model, both in the magnitude of C_p (specially at lower temperatures) and on the position of the maximum. This further reinforces the pressure correction of 400 bar when describing supercooled water. Importantly,

we note that despite the fact that the quantitative value of C_p cannot be provided in classical molecular dynamics simulations because nuclear quantum effects are neglected (only path integral calculations could lead to quantitative agreement as discussed in Ref. 93), the location of the maximum in C_p is remarkably well described by the pressure-shifted model. A very similar location for the maximum in C_p compared to that measured by Oguni and co-workers in water under confinement[91] has also been predicted in Ref. 20 using microdroplets. Nevertheless, despite the compatibility regarding the locus of the maximum, they significantly differ in their absolute values of C_p.

Next, we evaluate if the performance of the pressure-shifted TIP4P/Ice is also good for predicting the liquid density. In Fig. 3(a), we compare the available experimental data of the liquid density as a function of temperature for isobar ranging from 1 to 1600 bar[71,84] with the predicted ρ by the pressure-shifted TIP4P/Ice model. The agreement between experiments and simulations is quite impressive. A zoom-in view for the lowest temperatures as a function of pressure is also included in Fig. 3(b). Hence, for the first time, a water potential can simultaneously reproduce κ_T and ρ along pressure and supercooling (provided that the pressure shift is applied in the comparison between simulations and experiments). To the best of our knowledge, such good agreement between simulations and experiments for these two properties has never been achieved before. This overall improvement in the description of supercooled water by the TIP4P/Ice model further supports the need of applying a pressure shift on the model predictions.

To further test the predicting capability of the pressure-shifted TIP4P/Ice potential, we now evaluate the structural properties of liquid water. We start with A_2, a structural parameter that can be extracted from the oxygen–oxygen radial distribution function and that is related to the tetrahedrality of the local molecular environment.[64] More specifically, A_2 represents the number of excess oxygen atoms within a shell of a certain width containing the
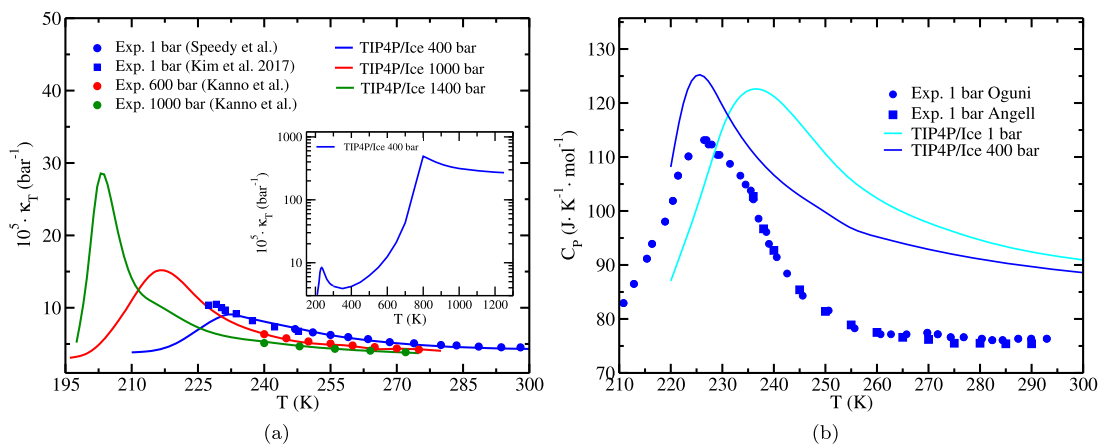
FIG. 2. (a) Isothermal compressibility as a function of temperature for different isobar as indicated in the legend. Colored symbols depict experimental results[18,21,94] while continuous curves correspond to data from the TIP4P/Ice water potential using system sizes of 500 water molecules. An inset showing the values of κ_T for the 400 bar isobar up to temperatures of 1200 K is also included. (b) Isobaric heat capacity as a function of temperature for different isobar as specified in the legend. Continuous curves correspond to simulation data using the TIP4P/Ice model and system sizes of 500 molecules whereas filled symbols indicate experimental measurements across the 1 bar isobar.[91,92]
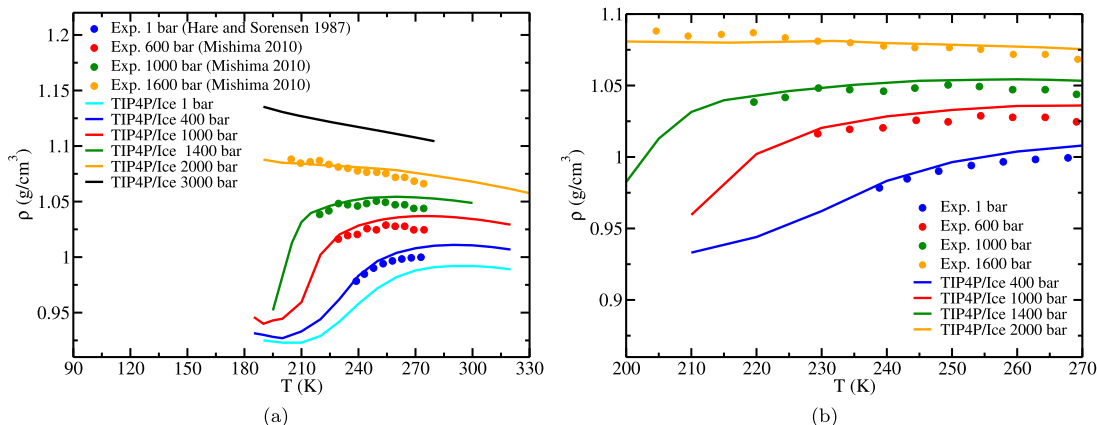
FIG. 3. (a) Density of liquid water as a function of temperature from TIP4P/Ice simulations using system sizes of 500 water molecules and experimental measurements[71,84] for different isobar as indicated in the legend. Experimental results at pressure p are compared to those of TIP4P/ICE at pressure $p + 400$ bar. (b) Zoom-in view of Panel (a) focusing on the moderately low temperature regime.

$g_{O-O}(r)$ second peak with respect to the average number of oxygen atoms within a spherical shell of the same width. A_2 can be evaluated as follows:

$$A_2 = 4\pi \int_{r_1}^{r_2} (g_{O-O}(r) - 1) r^2 dr, \qquad (3)$$

where r_1 and r_2 determine the beginning and the end of a shell containing the $g_{O-O}(r)$ second peak. The values of r_1 and r_2 have been extracted according to the methodology proposed in Ref. 64 for different water potentials such as the TIP4P/2005,[30] ST2,[95] mW,[36] SPC/E,[28] and iAMOEBA[32] models. Typically, the shell thickness of $r_2 - r_1$ is of the order of 1 Å, being the second maximum of $g_{O-O}(r)$

approximately located in the middle of such interval.[64] In Fig. 4(a), we show the results from the TIP4P/Ice shifted 400 bar and those experimentally reported at ambient pressure from Refs. 64 and 96. A remarkable agreement between experiments and modeling results is found.

Moreover, we explore the ability of TIP4P/Ice to predict g_2, the height of the second peak of the oxygen–oxygen radial distribution function.[97] In Fig. 4(b), we show the comparison of g_2 as a function of temperature and normal pressure from experiments at 1 bar[97] and TIP4P/Ice at 400 bar. Again, the correspondence between simulations and experiments is quite satisfactory. The main conclusion is that TIP4P/Ice represents unprecedentedly well supercooled water if the comparison is established between the experiment at pressure p and the model at $p + 400$ bar.
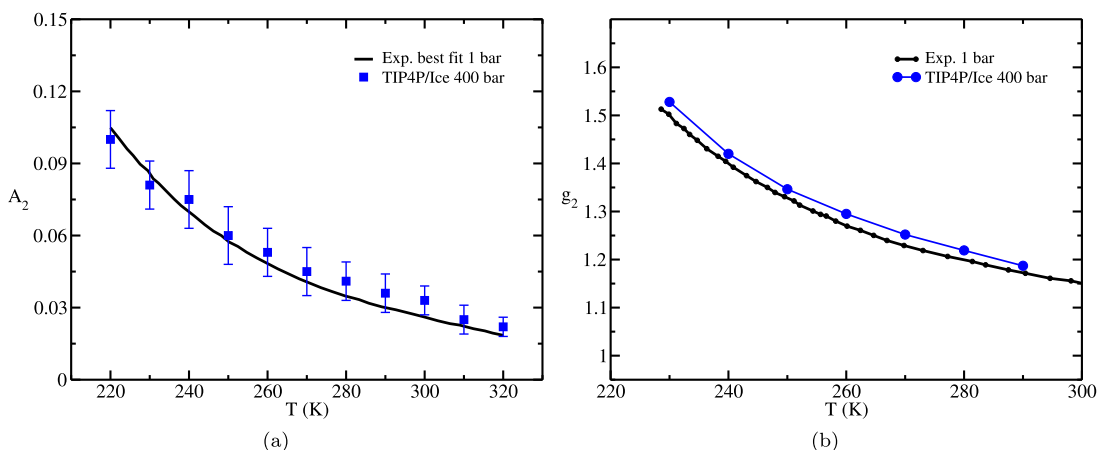
FIG. 4. (a) A_2 in nm³ [evaluated using Eq. (3)] as a function of temperature for the TIP4P/Ice potential at 400 bar (blue squares) and derived from experimental measurements of the liquid structure factor at normal pressure (black curve).[64,96] (b) Height of the second peak of the $g_{O-O}(r)$ as a function of temperature predicted by the TIP4P/Ice potential at 400 bar (blue circles) and from ultrafast x-ray experiments at ambient pressure (black circles).[97]

## D. Signatures of liquid–liquid immiscibility in TIP4P/Ice supercooled water

Once demonstrated that a 400 bar pressure shift on the TIP4P/Ice model can recapitulate the structural properties of supercooled water at ambient pressure as well as the isothermal compressibility and the liquid density for an impressive range of temperatures and pressures (Figs. 2–4), we focus on elucidating the physical behavior of the TIP4P/Ice potential under supercooled conditions, where experiments are hardly accessible.

In recent computational studies,[26,52–54] the existence of a liquid–liquid critical point in the TIP4P/Ice model has been proven. Indirect evidence of criticality is, indeed, the presence of maxima in κ_T in the supercooled regime [Fig. 2(a)]. In fact, if compressibility is determined for a given isobar (i.e., 400 bar) up to high temperatures (e.g., 1200 K), two maxima in κ_T can be observed [see the inset of Fig. 2(a)], which correspond to the liquid–liquid and liquid–vapor phase equilibria of the model. For the TIP4P/Ice model, the second maximum in compressibility along the 400 bar isobar, associated with the proximity of the liquid–vapor (LV) critical point, appears at about 800 K (i.e., 100 K above the LV critical temperature of the model). For the TIP4P/2005 potential, Gallo *et al.*[98] found a similar difference between the critical temperature of the model and the maximum in compressibility along this isobar. As expected, the height of the maximum in κ_T corresponding to the LV critical point is notably higher than that of the LLCP due to the much larger density difference between the two phases. However, the underlying thermodynamic explanation behind both κ_T maxima is identical: density fluctuations echoing phase separation of two immiscible phases.

In Fig. 5(a), the isothermal compressibility obtained along different isobar is shown. For some isobar, we have computed the isothermal compressibility using two system sizes, namely, 500 (empty circles) and 2000 (filled squares) molecules, obtaining consistent results. That suggests the absence of finite size effects in the fluctuations at least far from the critical point. Interestingly, we find that the highest compressibility maximum occurs at

1600 bar, hence suggesting that such pressure must be near the LLCP. At the critical point, the fluctuations should diverge in the thermodynamic limit although for finite systems the correlation length is limited by the size of the simulation box. Nonetheless, although the intensity of the response function maxima is affected by system size, their pressure–temperature location is expected to remain unchanged within the uncertainty of the calculations. In Fig. 5(b), we show the volume fluctuations as a function of time for a system formed by 500 molecules from which κ_T was computed at 196 K and 1600 bar; being this state the one at which we observe the highest value of compressibility among those studied (i.e., $48 \pm 4 \cdot 10^{-5}$ bar^{-1}). Note that for the 1700 bar isobar, the compressibility increases as the temperature decreases (reaching a value around $20 \pm 2 \cdot 10^{-5}$ bar^{-1} at 195 K). We were not able to determine κ_T at lower temperatures than 195 K since that would require runs of dozens of microseconds, which are beyond our computational resources. Therefore, we cannot state if the maximum in compressibility along 1700 bar would be lower or higher than that along 1600 bar. In any case, the large value of the compressibility found at 196 K and 1600 bar strongly suggests the proximity of the critical point of the model.

To have an overview of the thermodynamic behavior of the supercooled liquid in the TIP4P/Ice model, we perform a Maxwell construction using *NVT* simulations of 500 water molecules [Fig. 6(a)]. By plotting the obtained pressure from *NVT* simulations with different densities across several isotherms—ranging from 195 to 240 K and lasting between 1 and 3.5 μs—as a function of the system inverse density, we can estimate the approximate locus of the LLCP. The isotherms clearly develop a shoulder as temperature goes down. The data corresponding to the lowest temperatures (i.e., 195 and 200 K) are quite noisy due to the slow relaxation of water; however, they suggests the appearance of a non-monotonic behavior typical of phase coexistence in finite system sizes (a Van der Waals loop). This scenario is consistent with previous calculations situating the TIP4P/Ice LLCP at 189 K and 1725 bar[26] or at 188–203 K and 1500–1650 bar.[52] Furthermore, the scenario in
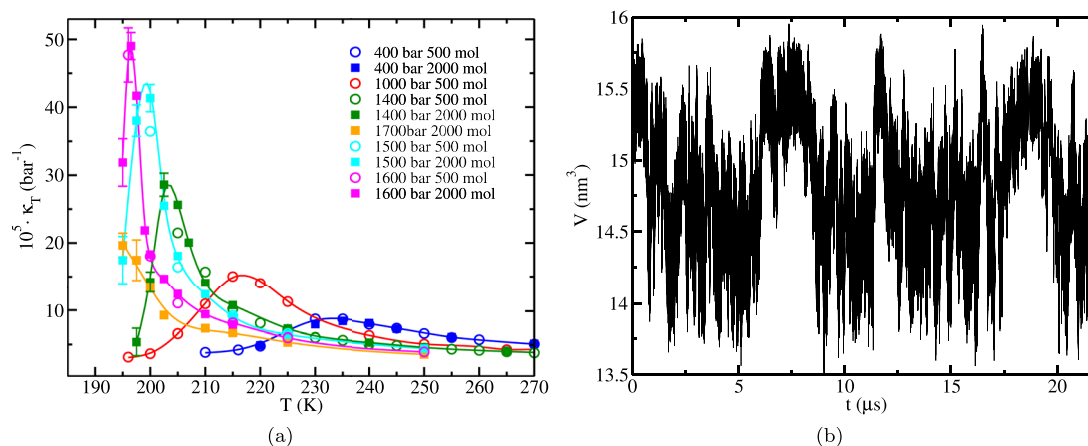
FIG. 5. (a) Isothermal compressibility as a function of temperature from TIP4P/Ice simulations using system sizes of 500 (empty circles) and 2000 (filled squares) molecules and for different isobar as indicated in the legend. (b) Time-evolution of the system volume for a 500-molecule system at 196 K and 1600 bar. The value of κ_T obtained from this run is $48 \pm 4 \cdot 10^{-5}$ bar^{-1}.
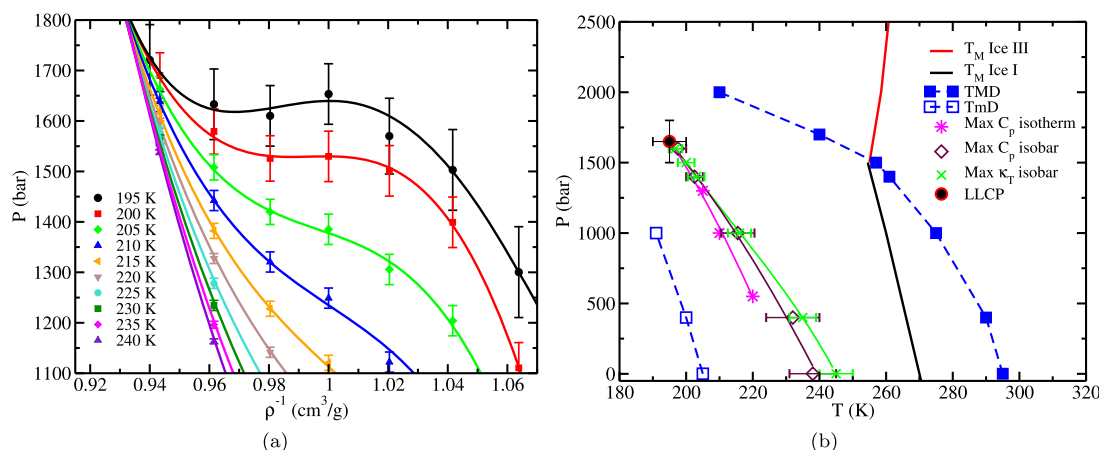
FIG. 6. (a) Computed pressure from *NVT* simulations of 500 TIP4P/Ice water molecules as a function of the inverse density for different isotherms as indicated in the legend. Continuous curves are cubic fits to the different values belonging to each isotherm. (b) Comprehensive scenario of the water anomalies in the TIP4P/Ice model. The loci of the temperature of maximum (TMD) and minimum (TmD) density for different isobar are represented by filled and empty blue squares, respectively. The maxima of the isothermal compressibility and isobaric heat capacity, found along isobar, and of the isobaric heat capacity, found along isotherms, are depicted by green crosses, brown diamonds, and purple asterisks, respectively. The location of the liquid–liquid critical point estimated through the convergence of the lines of the maxima in κ_T and C_p is represented by a red-black circle. Furthermore, the coexistence lines of water with ice Ih (T = 270 K, p = 1 bar; T = 265 K, p = 500 bar; T = 260 K, p = 1000 bar; and T = 254 K, p = 1500 bar) and ice III (T = 255 K, p = 1500 bar and T = 258.5 K, p = 2000 bar) are denoted by black and red lines, respectively.

Fig. 6(a) is also consistent with the compressibility maxima shown in Fig. 5(a).

To narrow down the location of the LLCP, we estimate the line of the maxima of the response functions, which in the vicinity of the LLCP coincides with the Widom line.[1,99] In Fig. 6(b), we plot the loci of the different maxima of the isothermal compressibility (green crosses) and the isobaric heat capacity (brown diamonds) along isobar as well as the maxima of C_p along isotherms (purple asterisks). The common point at which the extrapolations of all these lines converge is our estimate of the LLCP [Fig. 6(b)]. The critical temperature and pressure obtained through this approach are T_c = 195 ± 5 K and p_c = 1650 ± 150 bar. This estimation is consistent with our results presented in Fig. 6(a) and compatible with that of Debenedetti *et al.*[26] (within the statistical uncertainty) although a few degrees higher. Our estimate is also within the interval suggested by Škvára and Nezbeda.[52] In fact, this situation resembles that of the TIP4P/2005 potential where different estimates of the critical temperature differ by a few degrees.[26,55–57]

Interestingly, we can also observe in Fig. 6(b) that the loci of the temperature of maximum density (TMD, filled blue squares) and the temperature of minimum density (TmD, empty blue squares) embrace the estimated location of the LLCP, as previously shown for the TIP4P/2005,[58] ST2,[100] and TIP5P[59] models. In fact, a corresponding-state-like rescaling of pressure and temperature in these models has been shown to result in a significant degree of universality of this scenario [i.e., Fig. 6(b)] as well as in an intriguing correlation between the location of the liquid–liquid critical point and the rescaled locus of density extrema.[59] This scheme requires scaled coordinates of the extrema of the TMD lines (temperature and pressure) that are not yet available for the TIP4P/ICE. However, it would be interesting to test in the future if the TIP4P/ICE potential also follows the universal behavior shown in Ref. 59. Finally, from Fig. 6(b), we note that the LLCP is deeply buried

within the supercooled regime of the TIP4P/Ice model. Approximately 55–60 K of supercooling separate the locus of the LLCP from the ice–liquid melting line at 1650 bar [Fig. 6(b)]. Therefore, the spontaneous formation of ice nuclei within such region might be almost unavoidable unless extremely small sample sizes and/or short timescales are employed.[6–8] In contrast, the maxima in κ_T are separated with respect to the melting line by roughly 26 K at normal pressure, by 45 K at 1000 bar, and by almost 55 K at 1500 bar. Therefore, their experimental observation, especially at low pressures, should be more feasible as recently shown in Ref. 21.

E. Guidance for experimentally probing the liquid–liquid transition

In Sec. II C, we argue that the pressure-shifted TIP4P/Ice model could provide an approximate location for the experimental LLCP. Hence, by shifting 400 bar downward the TIP4P/Ice model LLCP obtained from our simulations (195 K and 1650 bar), we postulate the experimental location of the LLCP to be around 195 ± 5 K and 1250 ± 150 bar (shown with an empty circle in Fig. 7). This estimate for the experimental LLCP is not far away from other recent estimates. Hestand and Skinner[67] have suggested 204–210 K and p = 1000 bar after analyzing a series of experimental and simulation results. Moreover, Mishima and Sumita[101] have recently analyzed all experimental results for the equation of state of supercooled water, suggesting an experimental critical point at 207(5) K and 1050(90) bar [although a closer look to the results of Fig. 9(b) from this reference suggests 203(5) K and 1120(90) bar as a better option].

In this section, we discuss whether it is possible to experimentally probe the surroundings of the LLCP. The main hurdle is that the LLCP deeply lies in the ice stability region within the so-called *no man's land*,[102,103] where liquid water cannot supposedly exist due to unavoidable freezing. No man's land border, often referred to as
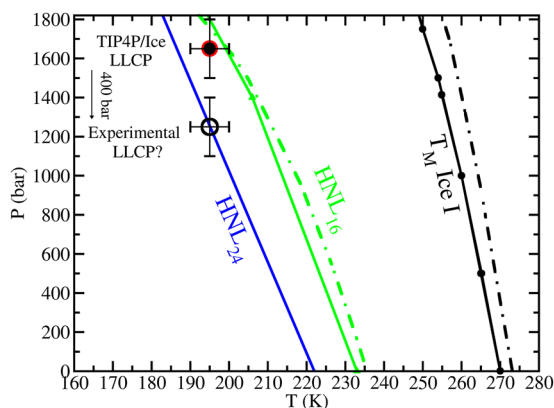
FIG. 7. Pressure–temperature location of the experimental (dashed–dotted lines) vs the TIP4P/Ice (solid lines) ice Ih melting (black line) and homogeneous nucleation (colored lines) lines. HNL subscripts indicate the rate (per cubic meter per second) to which the line of interest is associated. Experimental melting and HNL$_{16}$ lines are taken from Refs. 116 and 9, respectively. The simulation HNL$_{16}$ is taken from Refs. 108 and 117 (except for the 1400 bar point that has been interpolated in this work from the results in Refs. 108 and 117). The HNL$_{24}$ line (blue line, this work) crosses our guess for the experimental LLCP (empty circle) obtained after shifting 400 bar downward the TIP4P/Ice LLCP (solid circle).

the *homogeneous nucleation line* (HNL), is shown in dashed–dotted green line in Fig. 7. No man's land is the region at the left of the HNL, where the LLCP lies according to our prediction. The HNL was originally established for micrometric samples (or larger) cooled down at a few kelvin per minute.[24,104] With such experimental setup, the HNL corresponds to the loci where the nucleation rate, J, (the ice nucleation frequency per unit volume) is ~10^{16}/(m^{3}s) (J is approximately given by the cooling rate divided by the drop volume[105]). To stress the correspondence of the HNL with a certain nucleation rate, we refer to the HNL discussed in this paragraph as HNL$_{16}$.

In Fig. 7, we show the TIP4P/Ice HNL$_{16}$ line in solid green. Such line is obtained by finding, for a given pressure, the temperature at which J is equal to 10^{16}/(m^3 s). The TIP4P/Ice HNL$_{16}$ line is taken from our previous work where we studied homogeneous ice nucleation at 1 and 2000 bar[105] [here, we include an extra point at 1400 bar interpolated using Classical Nucleation Theory (CNT)[106,107] as explained later on in more detail]. Remarkably, the model (without pressure shift) predicts quite well both the experimental HNL$_{16}$ (solid vs dashed–dotted green lines) and the melting lines (solid vs dashed–dotted black lines). Even the fact that the HNL$_{16}$ has a more pronounced negative slope than the melting line is captured by the TIP4P/ICE.[9,105,108] We will therefore use the non-shifted model to evaluate ice nucleation rates in the surroundings of the LLCP to assess the viability of observing liquid–liquid equilibrium in water. We acknowledge that it is somewhat tricky to combine shifted with non-shifted predictions of the model. However, it seems that thermodynamic properties pertaining to water alone (i.e., density, compressibility, heat capacity, etc.) are nicely reproduced by the pressure-shifted model whereas those involving the liquid–ice transition (e.g., phase coexistence or ice nucleation rate) do not require a pressure shift. Considering that there is no model able to predict the overall

behavior of water, we believe that our approach of combining shifted and non-shifted results with the aforementioned criterion is a fair strategy to improve the accuracy of simulation predictions on the behavior of real water.

In order to gain access to the LLCP, it is necessary to shift no man's land border to lower temperatures, which can be achieved by probing higher nucleation rates (a higher rate corresponds to a lower temperature). It is possible to experimentally probe higher rates both by reducing the sample size and by increasing the cooling rate.[69] Using the $J(T)$ dependence of the model for several pressures (1, 1400, and 2000 bar), we find that the HNL that crosses our estimate for the possible experimental location of the LLCP corresponds to $J = 10^{24}$/(m^3 s) (drawn in solid blue in Fig. 7). The HNL$_{24}$ line corresponds to a rate eight orders of magnitude larger than the "traditional" HNL$_{16}$ border. Therefore, it seems a great challenge to devise an experimental setup that enables probing rates 10^8 times faster. It is encouraging that a few groups have already been able to measure nucleation rates in the range of 10^{24}–10^{30}/(m^3 s) at ambient pressure using nanometric drops and thin films.[6,8,109–111] In summary, our "recipe" to search for the LLCP is (i) look at the surroundings of 195 K and 1250 bar and (ii) keep the ratio between the cooling rate and the drop volume (see Ref. 105 for a detailed discussion about why this ratio is relevant), J, larger than 10^{24}/(m^3 s).

There are two limitations in this strategy. On the one hand, the cooling rate cannot be too high that equilibration of the liquid is not enabled. On the other hand, drops have to be large enough to display bulk behavior. It is as yet unclear whether surface effects in submicrometer volumes may overrun bulk behavior, which would be an insurmountable hurdle for the observation of the LLCP. However, the good accordance found in the nucleation rate between the TIP4P/Ice model (no surface) and experiments (surface) all the way from the microscopic to the nanoscopic drop regime[112] suggests that *bulk* nucleation rates can indeed be measured in nanodrop experiments.[6,8,109,111] Moreover, the experimental nucleation rate curve runs smoothly from low (microdroplets) to high (nanodroplets) supercooling, not showing any kink that could be indicative of a bulk-to-surface nucleation mechanism change.[112] Again, we insist on the fact that several groups have already probed rates of the order of 10^{24}/(m^3 s), circumventing the limitations here discussed at ambient pressures.[6,8,109–111] Extending these experiments[6,8,109,111] to high pressures would require other cooling methods than fast evaporation. Alternatively, since fast cooling under pressure is difficult, some recent experiments have shown that by means of an IR laser one can heat amorphous phases of water in a few picoseconds.[113–115] For instance, Nilsson and co-workers have heated an amorphous phase (at constant density) to a temperature around 200 K to study liquid water before it freezes. This has been performed by heating low-density amorphous (LDA)[113] or high-density amorphous (HDA) water[114] (in the latter followed by isothermal decompression of the sample). In both cases, spectroscopic evidence of phase separation between two liquids was found before the system froze (i.e., within timescales of around 1–100 μs).

F. Crystallization vs liquid metastability near the critical conditions

We now focus on the interplay between liquid metastability and crystallization in supercooled water under near-critical

conditions. To that aim, we select the isobar of 1400 bar. The choice of this pressure is motivated by the fact that although the critical pressure of TIP4P/Ice is around 1650 bar, the model reproduces the real liquid properties with a 400 bar shift, suggesting that the experimental critical point could be around 1250 bar. Thus, it seems reasonable to study ice formation for an intermediate pressure between these two values. Moreover, the ice nucleation rate barely changes for pressure variations of 200 bar.[118] We aim at computing J, which we do through the Classical Nucleation Theory (CNT) framework,[106,107]

$$J = \rho_l \sqrt{|\Delta\mu|/(6\pi k_B T N_c)} \left(\frac{24 D_l N_c^{2/3}}{\lambda^2} \right) \exp\left(-\Delta G_c / k_B T\right), \quad (4)$$

where ρ_l is the liquid number density, $\Delta\mu$ is the ice–liquid chemical potential difference, N_c is the number of molecules in the critical solid nucleus, D_l is the liquid diffusion coefficient, and λ is the average distance that a given water molecule diffuses to incorporate into the critical nucleus (typically of the order of 1 molecular diameter, i.e., 3–4 Å[119]). ΔG_c is the nucleation free energy barrier, which, according to CNT, is given by

$$\Delta G_c = \frac{16\pi \gamma_s^3}{3\rho_s^2 \Delta\mu^2}, \quad (5)$$

where γ_s is the interfacial free energy between the solid cluster and the liquid. We interpolate the value of the interfacial free energy (γ_s) at coexistence for a planar interface at 1400 bar from our previous work,[108] obtaining a value of $\gamma_s \sim 37$ mJ/m^2. We assume that γ_s varies with temperature along the isobar with the same slope as that found for both 1 and 2000 bar (i.e., an increase of γ_s of 0.285 mJ/m^2 per kelvin[108]). It should be mentioned that along an isobar the radius of the critical cluster also changes with the temperature. Then, we evaluate $\Delta\mu$ along temperature for the isobar of interest by performing thermodynamic integration of the molar enthalpy difference between both bulk (ice and liquid water) phases[120] obtained from liquid NpT simulations performed to compute κ_T (Fig. 2) and from NpT ice Ih bulk simulations run for this purpose.

By knowing J, we can estimate at 1400 bar the nucleation time (τ_J) as a function of supercooling ($\Delta T = T_{melting} - T$) for different system sizes. The nucleation time, or the time required for the appearance of a nucleus in a drop of volume V, is simply given by $1/(JV)$. In Fig. 8, we plot τ_J (dashed curves) for droplets of different radii (R) as a function of supercooling along the 1400 isobar. We also show (solid green line) the relaxation time (τ_r) that we define as the time required for a water molecule to diffuse its own molecular diameter (i.e., the time at which the mean squared displacement equals the squared diameter[69]). We acknowledge that there are more sophisticated approaches to estimate τ_r as through the intermediate scattering function $[F_s(Q,t)]$.[121] However, our definition is reasonable enough for the purpose of providing the order of magnitude in τ_r. We shall focus on analyzing the behavior of water at 60 K of supercooling (red dashed–dotted vertical line in Fig. 8) since that is the supercooling of the LLCP along the critical isobar (Fig. 7). As shown in Fig. 8, for droplets of radius 5 μm and 500 nm, nucleation events occur before the system can even equilibrate. Thereby, the equilibrium properties of water cannot be determined with these droplet sizes.[122] However, for droplets ranging from 5 to 50 nm (as those used in Refs. 6, 8, 109, and 111), the first nucleation event
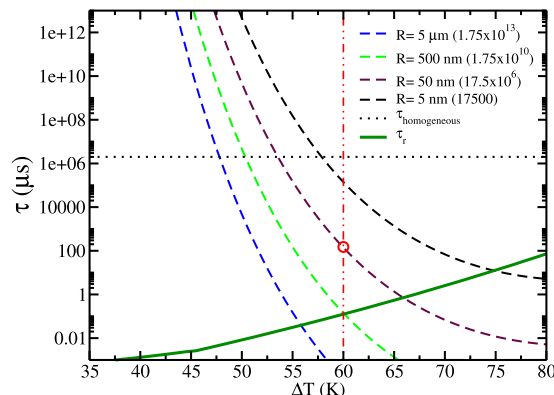
FIG. 8. Required time (τ_J) for nucleating ice within droplets of different radii as specified in the legend (dashed curves) and as a function of supercooling for a constant pressure of 1400 bar. The estimated number of water molecules for each droplet size is also included in the legend. The relaxation time (τ_r) (considered as the time for a water molecule to diffuse its own molecular diameter) is represented by a continuous green curve. The typical experimental timescale before observing nucleation in water microdroplets[9] is shown by a horizontal black dotted line, and the approximate supercooling at which the LLCP was found, is depicted by a vertical red dashed–dotted line.

occurs after 1 000 000 and 1000 relaxation times, respectively. Therefore, it should be possible to characterize the properties of metastable water employing systems of those sizes.

In Fig. 8, we also include a horizontal line depicting the typical observation timescale (of the order of seconds) for the microdroplet experiments, giving rise to the HNL$_{16}$ line (green curve in Fig. 7). Within this timescale and using droplets of $R = 5$ μm, one can only measure properties of water up to 47 K of supercooling at 1400 bar. Thus, according to the TIP4P/Ice model, one could not observe liquid–liquid demixing in such experiments. Nevertheless, by decreasing two orders of magnitude the size of the droplet (to 50 nm) and three orders of magnitude the observation timescale (down to milliseconds), the LLCP can be accessed. This would probably require extremely challenging setups: emulsions of water nanodroplets of about 50 nm and cooling rates of the order of 10^3–10^5 K/s. While such ultrafast cooling rates have been previously experimentally achieved at ambient pressure through vapor-phase supersonic expansions,[6,8] applying such fast cooling rates to nanoscopic droplets under pressure might be much more challenging (although they could be easily obtained in heating experiments).

We now evaluate the time required to freeze a sample. This is a key magnitude to take into consideration since in experiments ice is typically detected when the majority of the sample is frozen rather than when ice nuclei are initially formed.[108] While at moderate supercooling, the nucleation time is almost identical to that required to completely crystallize the sample, at very deep supercooling, it can be the ice growth rate what ultimately controls the crystallization timescale to freeze the droplet.[119,123] The Kolgomorov–Johnson–Mehl–Avrami (KJMA) equation[124–126] provides a useful framework to elucidate the interplay between nucleation and crystallization times for a given sample at very large supercooling. The KJMA expression introduces a new parameter (τ_x), which is the time required to crystallize a certain volume fraction of the sample (ϕ). τ_x is controlled by both the nucleation

rate (J) and the ice growth rate (u). We can evaluate τ_x through the KJMA expression:

$$\tau_x = ((3\phi)/(\pi J u^3))^{1/4}. \qquad (6)$$

For the purpose of evaluating τ_x, we have computed the ice growth rate (u) of the secondary prismatic plane of ice Ih as a function of supercooling for the isobar of 1400 bar [Fig. 9(a), blue circles]. Interestingly, we find that u increases with pressure, especially at lower temperatures, from 1 to 1400 bar. This observation is consistent with the fact that liquid water self-diffusion significantly increases upon compression up to moderate pressures of 2500–3000 bar.[127] In any case the difference becomes much smaller if u is plotted as a function of the supercooling as the melting temperature of the model is 255 K at 1400 bar and 270 K at 1 bar. We note

(a)

(b)
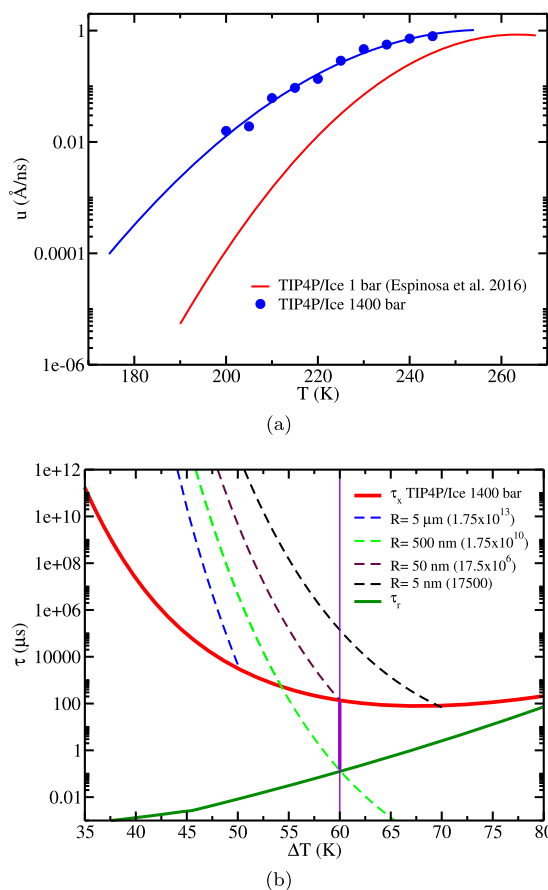
FIG. 9. (a) Growth rate of the ice Ih secondary prismatic plane as a function of temperature at normal pressure (red curve, data from Ref. [69]) and 1400 bar (blue circles, this work). (b) Time required for nucleating ice (τ_J) with droplets of different radii as specified in the legend (dashed curves) as a function of supercooling for 1400 bar. The estimated number of water molecules for each droplet size is included in the legend. The crystallization time, τ_x (or the time required for 70% of the volume to crystallize) for 1400 bar as a function of supercooling is depicted by a continuous red curve. The relaxation time (τ_r) is represented by a continuous green curve. Finally, the supercooling at which the LLCP could be found is depicted by a vertical purple line, whose thickest part indicates the time window available to measure 50 nm water drops in the liquid state.

that the experimental ice growth rate at 1 bar as a function of temperature is well described by the model.[69,128] Moreover, we have recently reported the existence of a maximum in the growth rate of the TIP4P/Ice model at normal pressure.[69,129] A similar behavior is expected at 1400 bar as the growth rate must go to zero when approaching the melting point at this pressure (i.e., around 255 K).

We plot τ_x as a function of the supercooling for the isobar of 1400 bar in Fig. 9(b) (red curve). We have used a value of $\phi = 0.7$ and employed the reported value of u for the secondary prismatic plane from Fig. 9(a) (which for our purpose provides a good enough estimate of the ice growth rate as shown in Ref. [130]). We notice that τ_x is almost constant for ϕ between 0.6 and 0.9 since τ_x changes as a power law of $\phi^{1/4}$. Remarkably, the minimum in τ_x is of the order of hundreds of microseconds, which is fully compatible with the experimental reported timescales before observing freezing in the employed samples to investigate liquid–liquid demixing in Refs. [113] and [114]. We note that the KJMA expression only contains intensive parameters such as J and u, and hence, it does not depend on the system size. Therefore, when the nucleation time is larger than τ_x, the traditional KJMA expression cannot be applied because the crystallization time is dominated by the nucleation time [Fig. 9(b), dashed curves], which is inversely proportional to the system's volume.[119,123] As the system size increases, the intersection between τ_J and τ_x moves toward smaller supercooling. Despite the KJMA expression being valid for all temperatures at the thermodynamic limit, for finite system sizes, it is certainly not the case. Thus, the required time to observe crystallization of the majority of a sample is given by the largest time of either τ_J or τ_x.

Overall, from Fig. 9(b), we find that beyond 75 K of supercooling it is not possible to equilibrate liquid water at 1400 bar as only extremely small droplets of less than 0.5 nm radius (where surface effects are dominant and there is no bulk water) could avoid freezing. Droplets of 500 nm at 60 K of supercooling would nucleate instantaneously (i.e., after 0.1 μs) without enough time to equilibrate [green dashed curve intersecting solid green line, Fig. 9(b)]. However, the crystallization of the sample induced by the emergence of multiple critical nuclei would not be experimentally detectable due to slow ice growth rate until hundreds of microseconds later (red line). As can be seen in Fig. 9(b), at 60 K of supercooling, the nucleation time is larger than both the relaxation time and τ_x for drops of 50 nm or smaller. Having these conditions satisfied, it is possible to measure thermodynamic liquid properties before freezing.

III. CONCLUSIONS

In this work, we show that the TIP4P/Ice model can accurately describe the experimental isothermal compressibility (Fig. 2) and liquid equation of state (Fig. 3) from 1 bar up to 1600 bar and low temperatures (down to 220 K) upon applying a pressure shift of 400 bar on its predicted thermodynamic magnitudes. Importantly, while other water force fields such as the iAMOEBA, TIP4P/2005, or MB-pol can successfully reproduce one of these two magnitudes at ambient pressure (i.e., iAMOEBA and TIP4P/2005 can recapitulate the liquid EOS, whereas the MB-pol can recapitulate the isothermal compressibility), they fail when describing the other thermodynamic property (Fig. 1). Furthermore, we compare structural features of liquid water at ambient pressure—such as the height and the integral of the second peak of the oxygen–oxygen radial distribution function—with the pressure-shifted model predictions

of the TIP4P/Ice. We obtain an outstanding agreement between experimental and modeling results for the tetrahedrality of liquid water as a function of supercooling (Fig. 4).

We perform a Maxwell construction to evaluate the existence and location of a liquid–liquid critical point in the TIP4P/Ice model. Our results confirm the location pinpointed by previous studies for the TIP4P/Ice model,[26,52] suggesting a locus around 195 ± 5 K and 1650 ± 150 bar for the second critical point (Fig. 6). Moreover, independent calculations of the maxima of the response functions (C_p and κ_T) also indicate a similar locus for the LLCP. Motivated by the resemblance between the pressure-shifted model and the experiment in the behavior of supercooled water, we propose an hypothetical location of the LLCP for real water slightly below 200 K and near 1250 bar.

Since such conditions are deeply buried within the supercooled regime of TIP4P/Ice water (Fig. 7), we assess the plausibility of gaining experimental access to the predicted LLCP location by probing metastable water before it freezes. We estimate the relaxation, nucleation, and crystallization timescales along an isobar near the critical pressure (Figs. 8 and 9). Our results strongly suggest that only droplets with radii around several tens of nanometers may serve to unravel the behavior of water at 60 K of supercooling, where liquid–liquid immiscibility may occur. Nevertheless, even with droplets of this size, freezing would take place in times of the order of the millisecond according to our simulations from Fig. 9. Therefore, the second critical point of water based on these considerations and assuming that real water would behave as TIP4P/Ice water, would only be accessible with an elaborate setup that enabled fast cooling and small volumes at moderate pressures. By using previous ice nucleation rate calculations,[108] we estimate the rate corresponding to the predicted location of the LLCP and obtain $J = 10^{24}/(\mathrm{m}^3 \mathrm{s})$. Therefore, our "recipe" for probing the LLCP would be searching using droplets of radius 50 nm or less in the surroundings of 195 K and 1250 bar while keeping the ratio between the cooling rate and the drop volume larger than $10^{24}/(\mathrm{m}^3 \mathrm{s})$. Remarkably, several experimental groups[6,8,109–111] have already measured homogeneous nucleation rates well beyond this value at ambient pressure with nanometric drops. Therefore, our results bring hope that the second critical point in water might be probed if similar experiments could be performed at pressures around 1250 bar.

ACKNOWLEDGMENTS

AUTHOR DECLARATIONS

Conflict of Interest

The authors have no conflicts to disclose.

Author Contributions

Jorge R. Espinosa: Conceptualization (equal); Data curation (equal); Formal analysis (equal); Funding acquisition (equal); Investigation (equal); Methodology (equal); Project administration (equal); Writing – original draft (equal); Writing – review & editing (equal). **Jose Luis F. Abascal**: Conceptualization (equal); Data curation (equal); Formal analysis (equal); Funding acquisition (equal); Investigation (equal); Methodology (equal); Project administration (equal); Writing – original draft (equal); Writing – review & editing (equal). **Lucia F. Sedano**: Conceptualization (equal); Data curation (equal); Formal analysis (equal); Funding acquisition (equal); Investigation (equal); Methodology (equal); Project administration (equal); Writing – original draft (equal); Writing – review & editing (equal). **Eduardo Sanz**: Conceptualization (equal); Data curation (equal); Formal analysis (equal); Funding acquisition (equal); Investigation (equal); Methodology (equal); Project administration (equal); Writing – original draft (equal); Writing – review & editing (equal). **Carlos Vega**: Conceptualization (equal); Data curation (equal); Formal analysis (equal); Funding acquisition (equal); Investigation (equal); Methodology (equal); Project administration (equal); Writing – original draft (equal); Writing – review & editing (equal).

DATA AVAILABILITY

The data that support the findings of this study are available within the article and from the corresponding author upon reasonable request.

REFERENCES

[1] P. G. Debenedetti, J. Phys.: Condens. Matter **15**, R1669 (2003).
[2] S. A. Zielke, A. K. Bertram, and G. N. Patey, J. Phys. Chem. B **119**, 9049 (2015).
[3] L. Lupi, A. Hudait, and V. Molinero, J. Am. Chem. Soc. **136**, 3156 (2014).
[4] R. Cabriolu and T. Li, Phys. Rev. E **91**, 052402 (2015).
[5] L. Ickes, A. Welti, C. Hoose, and U. Lohmann, Phys. Chem. Chem. Phys. **17**, 5514 (2015).
[6] A. Manka, H. Pathak, S. Tanimura, J. Wölk, R. Strey, and B. E. Wyslouzil, Phys. Chem. Chem. Phys. **14**, 4505 (2012).
[7] D. E. Hagen, R. J. Anderson, and J. L. Kassner, Jr., J. Atmos. Sci. **38**, 1236 (1981).
[8] A. J. Amaya and B. E. Wyslouzil, J. Chem. Phys. **148**, 084501 (2018).
[9] H. Kanno, R. J. Speedy, and C. A. Angell, Science **189**, 880 (1975).
[10] H. R. Pruppacher, J. Atmos. Sci. **52**, 1924 (1995).
[11] C. A. Stan, G. F. Schneider, S. S. Shevkoplyas, M. Hashimoto, M. Ibanescu, B. J. Wiley, and G. M. Whitesides, Lab Chip **9**, 2293 (2009).
[12] P. Taborek, Phys. Rev. B **32**, 5902 (1985).
[13] P. J. DeMott and D. C. Rogers, J. Atmos. Sci. **47**, 1056 (1990).
[14] B. Krämer, O. Hübner, H. Vortisch, L. Wöste, T. Leisner, M. Schwell, E. Rühl, and H. Baumgärtel, J. Chem. Phys. **111**, 6521 (1999).
[15] D. Duft and T. Leisner, Atmos. Chem. Phys. **4**, 1997 (2004).
[16] H. Laksmono, T. A. McQueen, J. A. Sellberg, N. D. Loh, C. Huang, D. Schlesinger, R. G. Sierra, C. Y. Hampton, D. Nordlund, M. Beye et al., J. Phys. Chem. Lett. **6**, 2826 (2015).
[17] C. A. Angell and J. C. Tucker, Science **181**, 342 (1973).
[18] R. J. Speedy and C. A. Angell, J. Chem. Phys. **65**, 851 (1976).
[19] S. Xu, G. W. Scherer, T. S. Mahadevan, and S. H. Garofalini, Langmuir **25**, 5076 (2009).
[20] H. Pathak, A. Späh, N. Esmaeildoost, J. A. Sellberg, K. H. Kim, F. Perakis, K. Amann-Winkel, M. Ladd-Parada, J. Koliyadu, T. J. Lane et al., Proc. Natl. Acad. Sci. U. S. A. **118**, e2018379118 (2021).

[21] K. H. Kim, A. Späh, H. Pathak, F. Perakis, D. Mariedahl, K. Amann-Winkel, J. A. Sellberg, J. H. Lee, S. Kim, J. Park, K. H. Nam, T. Katayama, and A. Nilsson, Science **358**, 1589 (2017).

[22] A. Späh, H. Pathak, K. H. Kim, F. Perakis, D. Mariedahl, K. Amann-Winkel, J. A. Sellberg, J. H. Lee, S. Kim, J. Park, K. H. Nam, T. Katayama, and A. Nilsson, Phys. Chem. Chem. Phys. **21**, 26 (2019).

[23] D. Liu, Y. Zhang, C.-C. Chen, C.-Y. Mou, P. H. Poole, and S.-H. Chen, Proc. Natl. Acad. Sci. U. S. A. **104**, 9570 (2007).

[24] O. Mishima and H. E. Stanley, Nature **396**, 329 (1998).

[25] P. H. Poole, F. Sciortino, U. Essmann, and H. E. Stanley, Nature **360**, 324 (1992).

[26] P. G. Debenedetti, F. Sciortino, and G. H. Zerze, Science **369**, 289 (2020).

[27] P. Gallo, K. Amann-Winkel, C. A. Angell, M. A. Anisimov, F. Caupin, C. Chakravarty, E. Lascaris, T. Loerting, A. Z. Panagiotopoulos, J. Russo *et al.*, Chem. Rev. **116**, 7463 (2016).

[28] H. J. C. Berendsen, J. R. Grigera, and T. P. Straatsma, J. Phys. Chem. **91**, 6269 (1987).

[29] W. L. Jorgensen, J. Chandrasekhar, J. D. Madura, R. W. Impey, and M. L. Klein, J. Chem. Phys. **79**, 926 (1983).

[30] J. L. F. Abascal and C. Vega, J. Chem. Phys. **123**, 234505 (2005).

[31] J. L. F. Abascal, E. Sanz, R. García Fernández, and C. Vega, J. Chem. Phys. **122**, 234511 (2005).

[32] J. W. Ponder, C. Wu, P. Ren, V. S. Pande, J. D. Chodera, M. J. Schnieders, I. Haque, D. L. Mobley, D. S. Lambrecht, R. A. DiStasio, Jr., *et al.*, J. Phys. Chem. B **114**, 2549 (2010).

[33] G. R. Medders, V. Babin, and F. Paesani, J. Chem. Theory Comput. **10**, 2906 (2014).

[34] P. M. Piaggi, A. Z. Panagiotopoulos, P. G. Debenedetti, and R. Car, J. Chem. Theory Comput. **17**, 3065 (2021).

[35] H. Chan, M. J. Cherukara, B. Narayanan, T. D. Loeffler, C. Benmore, S. K. Gray, and S. K. R. S. Sankaranarayanan, Nat. Commun. **10**, 379 (2019).

[36] V. Molinero and E. B. Moore, J. Phys. Chem. B **113**, 4008 (2009).

[37] B. Cheng, E. A. Engel, J. Behler, C. Dellago, and M. Ceriotti, Proc. Natl. Acad. Sci. U. S. A. **116**, 1110 (2019).

[38] S. Piana, A. G. Donchev, P. Robustelli, and D. E. Shaw, J. Phys. Chem. B **119**, 5113 (2015).

[39] P. M. Piaggi, J. Weis, A. Z. Panagiotopoulos, P. G. Debenedetti, and R. Car, Proc. Natl. Acad. Sci. **119**(33), e2207294119 (2022).

[40] B. Slater and A. Michaelides, Nat. Rev. Chem. **3**, 172 (2019).

[41] E. B. Moore and V. Molinero, Nature **479**, 506 (2011).

[42] I. Sanchez-Burgos, A. R. Tejedor, C. Vega, M. M. Conde, E. Sanz, J. Ramirez, and J. R. Espinosa, J. Chem. Phys. **157**, 094503 (2022).

[43] A. Garkul and V. Stegailov, Sci. Rep. **12**, 13325 (2022).

[44] Y. Liu, J. C. Palmer, A. Z. Panagiotopoulos, and P. G. Debenedetti, J. Chem. Phys. **137**, 214505 (2012).

[45] F. Sciortino, I. Saika-Voivod, and P. H. Poole, Phys. Chem. Chem. Phys. **13**, 19759 (2011).

[46] J. C. Palmer, F. Martelli, Y. Liu, R. Car, A. Z. Panagiotopoulos, and P. G. Debenedetti, Nature **510**, 385 (2014).

[47] J. C. Palmer, A. Haji-Akbari, R. S. Singh, F. Martelli, R. Car, A. Z. Panagiotopoulos, and P. G. Debenedetti, J. Chem. Phys. **148**, 137101 (2018).

[48] D. T. Limmer and D. Chandler, J. Chem. Phys. **135**, 134503 (2011).

[49] D. T. Limmer and D. Chandler, J. Chem. Phys. **138**, 214504 (2013).

[50] J. Weis, F. Sciortino, A. Z. Panagiotopoulos, and P. G. Debenedetti, J. Chem. Phys. **157**, 024502 (2022).

[51] J. L. F. Abascal and C. Vega, J. Chem. Phys. **133**, 234502 (2010).

[52] J. Škvára and I. Nezbeda, J. Mol. Liq. **367**, 120508 (2022).

[53] R. Foffi, J. Russo, and F. Sciortino, J. Chem. Phys. **154**, 184506 (2021).

[54] R. S. Singh, J. C. Palmer, A. Z. Panagiotopoulos, and P. G. Debenedetti, J. Chem. Phys. **150**, 224503 (2019).

[55] T. Sumi and H. Sekino, RSC Adv. **3**, 12743 (2013).

[56] R. S. Singh, J. W. Biddle, P. G. Debenedetti, and M. A. Anisimov, J. Chem. Phys. **144**, 144504 (2016).

[57] T. Yagasaki, M. Matsumoto, and H. Tanaka, Phys. Rev. E **89**, 020301(R) (2014).

[58] M. A. González, C. Valeriani, F. Caupin, and J. L. F. Abascal, J. Chem. Phys. **145**, 054505 (2016).

[59] B. Uralcan, F. Latinwo, P. G. Debenedetti, and M. A. Anisimov, J. Chem. Phys. **150**, 064503 (2019).

[60] R. Foffi and F. Sciortino, J. Phys. Chem. B **127**, 378–386 (2023).

[61] J. C. Palmer, P. H. Poole, F. Sciortino, and P. G. Debenedetti, Chem. Rev. **118**, 9129 (2018).

[62] A. Jedrecy, A. M. Saitta, and F. Pietrucci, J. Chem. Phys. **158**, 014502 (2023).

[63] T. E. Gartner III, K. M. Hunter, E. Lambros, A. Caruso, M. Riera, G. R. Medders, A. Z. Panagiotopoulos, P. G. Debenedetti, and F. Paesani, J. Phys. Chem. Lett. **13**, 3652 (2022).

[64] H. Pathak, J. C. Palmer, D. Schlesinger, K. T. Wikfeldt, J. A. Sellberg, L. G. M. Pettersson, and A. Nilsson, J. Chem. Phys. **145**, 134507 (2016).

[65] T. E. Gartner III, L. Zhang, P. M. Piaggi, R. Car, A. Z. Panagiotopoulos, and P. G. Debenedetti, Proc. Natl. Acad. Sci. U. S. A. **117**, 26040 (2020).

[66] T. E. Gartner III, P. M. Piaggi, R. Car, A. Z. Panagiotopoulos, and P. G. Debenedetti, Phys. Rev. Lett. **129**, 255702 (2022).

[67] N. J. Hestand and J. L. Skinner, J. Chem. Phys. **149**, 140901 (2018).

[68] J. L. F. Abascal and C. Vega, J. Chem. Phys. **134**, 186101 (2011).

[69] J. R. Espinosa, C. Navarro, E. Sanz, C. Valeriani, and C. Vega, J. Chem. Phys. **145**, 211922 (2016).

[70] Y. Ni and J. L. Skinner, J. Chem. Phys. **144**, 214501 (2016).

[71] O. Mishima, J. Chem. Phys. **133**, 144503 (2010).

[72] D. A. Fuentevilla and M. A. Anisimov, Phys. Rev. Lett. **97**, 195702 (2006).

[73] H. Kanno and K. Miyata, Chem. Phys. Lett. **422**, 507 (2006).

[74] H. E. Stanley, C. A. Angell, U. Essmann, M. Hemmati, P. H. Poole, and F. Sciortino, Physica A **205**, 122 (1994).

[75] S. L. Bore, P. M. Piaggi, R. Car, and F. Paesani, J. Chem. Phys. **157**, 054504 (2022).

[76] J. R. Espinosa, C. Vega, and E. Sanz, J. Phys. Chem. C **120**, 8068 (2016).

[77] A. Haji-Akbari and P. G. Debenedetti, Proc. Natl. Acad. Sci. U. S. A. **112**, 10582 (2015).

[78] H. Niu, Y. I. Yang, and M. Parrinello, Phys. Rev. Lett. **122**, 245501 (2019).

[79] U. Essmann, L. Perera, M. L. Berkowitz, T. Darden, H. Lee, and L. G. Pedersen, J. Chem. Phys. **103**, 8577 (1995).

[80] B. Hess, H. Bekker, H. J. C. Berendsen, and J. G. E. M. Fraaije, J. Comput. Chem. **18**, 1463 (1997).

[81] B. Hess, C. Kutzner, D. Van Der Spoel, and E. Lindahl, J. Chem. Theory Comput. **4**, 435 (2008).

[82] G. Bussi, D. Donadio, and M. Parrinello, J. Chem. Phys. **126**, 014101 (2007).

[83] M. Parrinello and A. Rahman, J. Appl. Phys. **52**, 7182 (1981).

[84] D. E. Hare and C. M. Sorensen, J. Chem. Phys. **87**, 4840 (1987).

[85] V. Holten, J. V. Sengers, and M. A. Anisimov, J. Phys. Chem. Ref. Data **43**, 043101 (2014).

[86] V. Holten, D. T. Limmer, V. Molinero, and M. A. Anisimov, J. Chem. Phys. **138**, 174501 (2013).

[87] K. A. Motakabbir and M. Berkowitz, J. Phys. Chem. **94**, 8359 (1990).

[88] H. L. Pi, J. L. Aragones, C. Vega, E. G. Noya, J. L. F. Abascal, M. A. Gonzalez, and C. McBride, Mol. Phys. **107**, 365 (2009).

[89] T. Bryk and A. D. J. Haymet, Mol. Simul. **30**, 131 (2004).

[90] L.-P. Wang, T. Head-Gordon, J. W. Ponder, P. Ren, J. D. Chodera, P. K. Eastman, T. J. Martinez, and V. S. Pande, J. Phys. Chem. B **117**, 9956 (2013).

[91] S. Maruyama, K. Wakabayashi, and M. Oguni, AIP Conf. Proc. **708**, 675–676 (2004).

[92] C. A. Angell, W. J. Sichina, and M. Oguni, J. Phys. Chem. **86**, 998 (1982).

[93] C. Vega, M. M. Conde, C. McBride, J. L. F. Abascal, E. G. Noya, R. Ramírez, and L. M. Sesé, J. Chem. Phys. **132**, 046101 (2010).

[94] H. Kanno and C. A. Angell, J. Chem. Phys. **70**, 4008 (1979).

[95] F. H. Stillinger and A. Rahman, J. Chem. Phys. **60**, 1545 (1974).

[96] L. B. Skinner, C. J. Benmore, J. C. Neuefeind, and J. B. Parise, J. Chem. Phys. **141**, 214507 (2014).

[97] J. A. Sellberg, C. Huang, T. A. McQueen, N. D. Loh, H. Laksmono, D. Schlesinger, R. G. Sierra, D. Nordlund, C. Y. Hampton, D. Starodub *et al.*, Nature **510**, 381 (2014).

[98] P. Gallo, D. Corradini, and M. Rovere, Nat. Commun. **5**, 5806 (2014).

[99] G. Franzese and H. E. Stanley, J. Phys.: Condens. Matter **19**, 205126 (2007).

[100] P. H. Poole, I. Saika-Voivod, and F. Sciortino, J. Phys.: Condens. Matter **17**, L431 (2005).

[101] O. Mishima and T. Sumita, J. Phys. Chem. B **127**, 1414 (2023).

[102] P. H. Handle, T. Loerting, and F. Sciortino, Proc. Natl. Acad. Sci. U. S. A. **114**, 13336 (2017).

[103] F. Caupin, J. Non-Cryst. Solids **407**, 441 (2015).

[104] C. A. Angell, "Supercooled water," Annu. Rev. Phys. Chem. **34**(1), 593–630 (1983).

[105] J. R. Espinosa, A. Zaragoza, P. Rosales-Pelaez, C. Navarro, C. Valeriani, C. Vega, and E. Sanz, Phys. Rev. Lett. **117**, 135702 (2016).

[106] M. Volmer and A. Weber, Z. Phys. Chem. **119U**, 277 (1926).

[107] R. Becker and W. Döring, Ann. Phys. **416**, 719 (1935).

[108] V. Bianco, P. Montero de Hijes, C. P. Lamas, E. Sanz, and C. Vega, Phys. Rev. Lett. **126**, 015704 (2021).

[109] A. Bhabhe, H. Pathak, and B. E. Wyslouzil, J. Phys. Chem. A **117**, 5472 (2013).

[110] Y. Xu, N. G. Petrik, R. S. Smith, B. D. Kay, and G. A. Kimmel, J. Phys. Chem. Lett. **8**, 5736 (2017).

[111] J. Huang and L. S. Bartell, J. Phys. Chem. **99**, 3924 (1995).

[112] J. R. Espinosa, C. Vega, and E. Sanz, J. Phys. Chem. C **122**, 22892 (2018).

[113] K. Amann-Winkel, K. H. Kim, N. Giovambattista, M. Ladd-Parada, A. Späh, F. Perakis, H. Pathak, C. Yang, T. Eklund, T. J. Lane *et al.*, Nat. Commun. **14**, 442 (2023).

[114] K. H. Kim, K. Amann-Winkel, N. Giovambattista, A. Späh, F. Perakis, H. Pathak, M. L. Parada, C. Yang, D. Mariedahl, T. Eklund *et al.*, Science **370**, 978 (2020).

[115] L. Kringle, W. A. Thornley, B. D. Kay, and G. A. Kimmel, Science **369**, 1490 (2020).

[116] P. W. Bridgman, Proc. Am. Acad. Arts Sci. **47**, 441 (1912).

[117] J. R. Espinosa, A. L. Diez, C. Vega, C. Valeriani, J. Ramirez, and E. Sanz, Phys. Chem. Chem. Phys. **21**, 5655 (2019).

[118] P. M. de Hijes, J. R. Espinosa, C. Vega, and C. Dellago, J. Chem. Phys. **158**, 124503 (2023).

[119] J. R. Espinosa, E. Sanz, C. Valeriani, and C. Vega, J. Chem. Phys. **141**, 18C529 (2014).

[120] C. Vega, E. Sanz, J. L. F. Abascal, and E. G. Noya, J. Phys.: Condens. Matter **20**, 153101 (2008).

[121] P. Gallo, F. Sciortino, P. Tartaglia, and S.-H. Chen, Phys. Rev. Lett. **76**, 2730 (1996).

[122] D. T. Limmer and D. Chandler, Mol. Phys. **113**, 2799 (2015).

[123] B. A. Berg and S. Dubey, Phys. Rev. Lett. **100**, 165702 (2008).

[124] A. N. Kolmogorov, Isz. Akad. Nauk SSR, Ser. Fiz. **3**, 355 (1937).

[125] W. A. Johnson and R. F. Mehl, Trans. Am. Inst. Min., Metall. Pet. Eng. **135**, 416 (1939).

[126] M. Avrami, J. Chem. Phys. **8**, 212 (1939).

[127] P. Montero de Hijes, E. Sanz, L. Joly, C. Valeriani, and F. Caupin, J. Chem. Phys. **149**, 094503 (2018).

[128] Y. Xu, N. G. Petrik, R. S. Smith, B. D. Kay, and G. A. Kimmel, Proc. Natl. Acad. Sci. U. S. A. **113**, 14921 (2016).

[129] P. Montero de Hijes, J. R. Espinosa, C. Vega, and E. Sanz, J. Chem. Phys. **151**, 044509 (2019).

[130] D. Rozmanov and P. G. Kusalik, J. Chem. Phys. **137**, 094702 (2012).